On the Properties of Methylbenzoate/*n*-Hexane Mixed Solvents: A Theoretical and Experimental Study

Santiago Aparicio,* Rafael Alcalde, María J. Dávila, Begoña García, and José M. Leal

Departamento de Química, Universidad de Burgos, 09001 Burgos, Spain

Received: April 27, 2007; In Final Form: February 12, 2008

This paper reports on an experimental and theoretical study of methylbenzoate/*n*-hexane mixed solvents as a function of pressure and temperature in the whole composition range. We have measured the pressure−volume−temperature (PVT) behavior of these fluids over wide temperature and pressure ranges; from the experimental data, relevant derived coefficients required for the fluid's characterization were calculated. The structure of mixed fluids was analyzed from macroscopic data according to excess and mixing properties. The statistical associating fluid theory (SAFT) and perturbed chain (PC)-SAFT molecularly based equations of state were used to predict the PVT behavior with model parameters for pure fluids fitted from correlation of available saturation literature data. The results provided by the PC-SAFT equation of state were clearly superior. Using the fitted PC-SAFT parameters, the global phase behavior of the mixture was predicted, and a type I pattern was inferred according to the van Konynenburg systematic. The molecular level structure was studied through classical molecular dynamics simulations in the NPT ensemble using the optimized potential for liquid simulations (*all atom* version) (OPLS-AA) force field. Molecular dynamics provides, on one hand, theoretical values of thermophysical properties, which are compared with the experimental ones to check the quality of simulations, and, on the other hand, valuable molecular level structural and dynamic information. Based on both macroscopic and microscopic studies, fluid structure was inferred.

1. Introduction

The study of the properties and structure of complex liquid mixtures is necessary for both theoretical and practical reasons.[1] Mixed solvents are almost ubiquitous in the industry in very different fields ranging from petrochemistry to pharmaceutical industries.[2] The development and design of industrial processes requires the selection of the most adequate solvent for each application to increase the productivity, reduce the waste, and improve the whole product cycle, according to the demand of sustainable and environmentally friendly technologies.[3]

For efficient process design, the macroscopic thermophysical properties of mixed fluids have to be known accurately a priori for the enormous amount of candidate fluids and in wide pressure−temperature ranges.[4] Although the experimental determination of these properties is the obvious and more reliable choice, it is not feasible to measure all the properties for all the required systems because of economical and time constraints,[5] and thus, other alternatives have to be considered.

Macroscopic properties are related to molecular level structure and intermolecular interactions. Thus, statistical mechanics allows the prediction and correlation of these properties, but a detailed knowledge of fluid structure is required. Remarkable advances have been carried out in theoretical modeling of liquids in recent years, through both molecular simulation and modern molecular based equations of state, allowing the prediction of complex liquid behavior with variable accuracy depending on the nature of the considered systems. However, many of the available approaches consider simplified views of liquid structure or even include semiempirical parameters with physical meaning not fully clarified. The extremely complex nature of intermolecular interactions in the liquid state is poorly described by most of the available theoretical models. Hence, the relationships among micro- and macroscopic properties are not fully understood.[6] Among the different approaches available to circumvent this problem, the development of combined experimental−theoretical studies on key systems, selected in a systematic way, provides a close view on the connections among macroscopic and microscopic features. Thus, a deeper insight into the molecular structure−macroscopic properties relationships can be extracted.[7]

The accurate determination of thermophysical properties as a function of pressure and temperature is extremely consuming, both in time and economical resources, and state-of-the-art apparatus are required. Nevertheless, this is the only reliable way to obtain these properties to test the theoretical predictions and validate the available models. Although certain molecular information may be inferred from macroscopic properties, at least in a qualitative way, this is not always easy or direct. On the other hand, molecular modeling studies provide the molecular information required, which may be tested against the macroscopic data. Hence, both approaches are complementary. Thus, the objective of this combined approach is to measure now to avoid measurements in the future.

The stated methodology has been applied in previous works to characterize selected families of molecules.[8] It is considered in this work for the study of methylbenzoate (MB)/*n*-hexane (HEX) binary liquid mixtures in the whole composition range as a function of pressure and temperature. MB, Figure 1, is a representative member of the aromatic esters family with a wide number of remarkable technological applications.[8c] The presence of the polarizable aromatic π-electron system near the dipolar

* To whom correspondence should be addressed. E-mail: sapar@ubu.es.

10.1021/jp073247s CCC: $40.75
Published on Web 03/29/2008

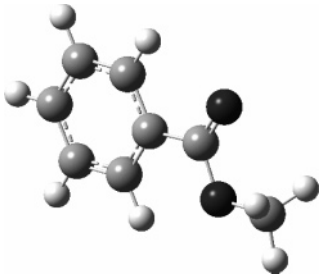

Figure 1. Optimized gas-phase structure of MB calculated at the B3LYP/6-311++g** theoretical level.[8c] Color code: black = oxygen, dark gray = carbon, and white = hydrogen.

ester group, together with their hydrophobic and aprotic character, confers these molecules a highly selective solvent ability. Few studies have been reported on benzoate containing mixtures, with most of them being at ambient pressure conditions.[9] Thus, as a continuation of our previous works,[10] in which systematic studies have been reported for selected key benzoate containing mixtures, the studies are extended to high-pressure conditions to characterize and analyze the behavior of mixed fluids in the whole pressure−volume−temperature (PVT) space.

The modeling of PVT behavior of fluids is commonly done by use of equations of state (EOS), which are efficient and simple tools for the representation of the PVT properties over wide ranges of pressure and temperature.[11]Although literally hundreds of EOS have been put forward with variable degrees of success, only molecularly based EOS have enough theoretical background and can separate the interactions and quantify the effects of the fluid's structure on bulk properties and phase behavior. EOS based on Wertheim's perturbation theory[12] have received growing recognition, both in academia and industry, giving rise to a set of EOS known as statistical associating fluid theory (SAFT). The original SAFT approach was developed by Chapman and colloborators,[13a,b] but a slightly different version developed by Huang and Radosz (so−called engineering version)[13c] reached wide acceptance and has been thoroughly applied for systems of very different natures since its publication. The new versions of SAFT family EOS (second-generation) have proven better performance than the original one; thus, the perturbed chain (PC)-SAFT[14] version was applied in this work for the studied system, and the results were compared with the Huang and Radosz engineering SAFT. We may expect, as we will see afterward, better predictions for PC-SAFT than for the original SAFT. However, this comparison is still useful because the original SAFT model is included in many process simulators, and thus, the study of its performance is still important.

Finally, this work includes classical molecular dynamics (MD) simulations in the NPT ensemble according to the optimized potential for liquid simulations (*all atom* version) (OPLS-AA) force field for different temperatures, pressures, and compositions.[15] MD provides predictions of macroscopic properties, such as density, which are compared with experimental ones to test the simulation's reliability, together with valuable structural information, analyzed according to radial distribution functions (RDF) of selected pairs. The fluid dynamics also was studied through the calculated self−diffusion coefficients and the mean square displacements of the mixtures.

2. Materials and Methods

2.1. Solvents and Mixture Preparation. MB (99.9% GC purity) and HEX (99.7% GC purity) were purchased from Fluka and stored out of light over Fluka Union Carbide 0.4 nm molecular sieves to avoid moisture absorption. Before measurements, fluids were degassed with ultrasound and used without further purification. Binary liquid mixtures were prepared by syringing amounts, weighed to $\Delta m = \pm 1 \times 10^{-5}$ g with a Mettler AT 261 Delta Range balance, into suitably stoppered bottles to avoid preferential evaporation. The estimated accuracy of the molar fraction was $\pm 1 \times 10^{-4}$.

2.2. Instruments and Procedures. The apparatus used in the PVT measurements was previously described in detail.[16] The system is installed around a high-pressure vibrating tube densimeter. The cell temperature was controlled by a Julabo F32 circulating bath; a Pt100 platinum sensor located in the measuring cell connected to a AΣΔF250 unit measures the temperature to $\pm 1 \times 10^{-2}$ K. The system pressure was controlled and measured by a Ruska 7615 Digital Pressure controller. The pressure was kept constant to $\pm 5 \times 10^{-3}$ MPa by the controller and measured to $\pm 1 \times 10^{-2}$ MPa with a pressure sensor. The pressurizing fluid was separated from the sample by a high-pressure liquid-to-liquid separator (Pressurements T3600E) that contains a Teflon diaphragm to send out the pressure. The pressure transducer and thermometer were previously calibrated through well-defined and traceable procedures. A 14-parameter equation was used[16] for proper apparatus calibration, with toluene (Fluka, 99.7%) and water (Millipore, resistivity 18.2 mΩ cm) as reference fluids.[17] Density measurements through vibrating tube apparatus are affected in a certain manner by the sample viscosity,[8c] but considering the low viscosity of the studied mixtures no corrections were included in the reported data because these would be below the accuracy limit. Thus, an accuracy of $\pm 1 \times 10^{-4}$ g·cm^{-3} can be inferred for experimental raw density data.

2.3. Classical Molecular Dynamics Simulations. Simulations were carried out using the TINKER molecular modeling package.[18] All simulations were performed in the NPT ensemble; the Nosé−Hoover method[19] was used to control the temperature and pressure of the studied systems. The motion equations were solved using the Verlet leapfrog integration algorithm.[20] The molecular geometries were restrained according to the SHAKE algorithm.[21] Long-range electrostatic interactions were treated with the smooth particle mesh Ewald method.[22] The simulated systems consist of cubic boxes with 250 total molecules to which periodic boundary conditions were applied in three directions. The initial liquid box sizes were established according to the experimental densities. Simulations were performed using a cutoff $L/2$ Å radius for the nonbonded interactions, with L being the box side. Initial configurations were generated using the PACKMOL program[23a] that uses the BOX-QUACAN[23b] local-minimization method to obtain adequate starting configurations. These boxes were minimized according to the MINIMIZE program in the TINKER package to a 0.01 kcal mol^{-1} Å^{-1} root mean square (rms) gradient. Several heating and quenching steps in the NVT ensemble up to 500 K were then performed, after which a 100 ps NVT equilibration molecular dynamics simulation was run at the studied temperature. Finally, from the output NVT simulation configuration, a run of 500 ps (time step 1 fs) in the NPT ensemble at the selected temperature and pressure was run, from which the first 100 ps were used to ensure equilibration (checked through constant energy) and the remaining 400 ps were used for data collection. OPLS-AA[15] was used to mimic both molecules. Merz−Singh−Kollman (MK)[24]charges for MB previously obtained through B3LYP/6-311++g** calculations were used in all the simulations.[8c]

3. Results and Discussion

3.1. Thermophysical Study. Experimental compressed liquid densities of MB/HEX mixed solvents in the 278.15−358.15 K

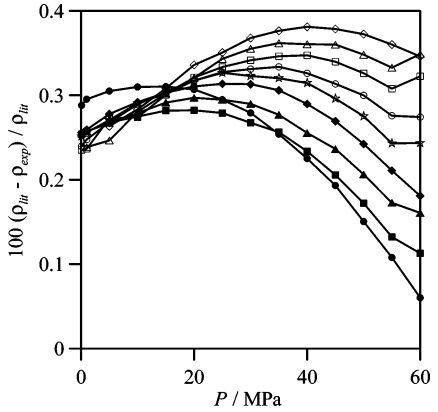

Figure 2. Relative deviations between experimental *n*-hexane readings and literature data.[17] (●) 278.15 K, (■) 288.15 K, (▲) 298.15 K, (◆) 308.15 K, (★) 318.15 K, (○) 328.15 K, (□) 338.15 K, (△) 348.15 K, and (◇) 358.15 K. (—) Trend lines for guiding purposes.

and 0.1−60 MPa ranges are listed in Table S1 in the Supporting Information. These data were correlated with temperature and pressure according to the TRIDEN 10-parameter equation,[25] which combines the modified Rackett equation for saturation densities with Tait's equation for isothermal compressed densities, eqs 1−3:

$$\rho_0 = \frac{A_R}{B_R^{[1+(1-T/C_R)D_R]}} \quad (1)$$

$$\rho = \frac{\rho_0}{1 - C_T \ln\dfrac{B_T + P}{B_T + P_0}} \quad (2)$$

$$B_T = b_0 + b_1\frac{T}{E_T} + b_2\left(\frac{T}{E_T}\right)^2 + b_3\left(\frac{T}{E_T}\right)^3 \quad (3)$$

The reference pressure $P_0 = 0.1$ MPa was used at all temperatures, and the corresponding reference densities, ρ_0, were correlated with eq 1, with the C_T Tait parameter being temperature-independent. The correlation parameters were deduced using a Levenberg−Marquardt least-squares algorithm, and the optimal fitting was assessed by the absolute average percentage deviation (AAD), eq 4:

$$\mathrm{AAD} = \frac{100}{N}\sum_{j=1}^{N}\left|\frac{\rho_{i,\mathrm{EXP}} - \rho_{i,\mathrm{CAL}}}{\rho_{i,\mathrm{EXP}}}\right| \quad (4)$$

where N is the number of data-pairs. Table S2 in the Supporting Information summarizes the fitting parameters deduced. From the TRIDEN fit of experimental densities, isobaric expansivity, isothermal compressibility, and internal pressure were calculated according to well-known thermodynamic relations[16a] (Tables S3−S5 in the Supporting Information). Excess properties were calculated considering the ideality criteria previously reported.[16a] The accuracy of our results may be inferred from Figure 2 in which HEX densities obtained in this work are compared with those from the literature. Low deviations (average deviation = 0.28%) are obtained in the pressure−temperature range considered, showing the good performance of the instrument and procedures. Experimental and calculated data are plotted in Figures 3−7for isothermal and isobaric conditions to analyze separately the pressure and temperature effects on mixture properties.

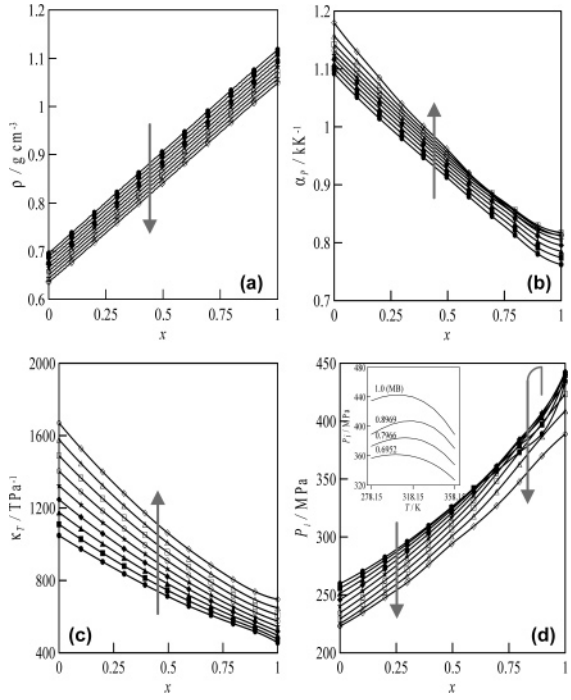

Figure 3. Temperature effect on the isobaric properties at $P = 30$ MPa for the x MB + $(1 - x)$ *n*-hexane binary system. (a) Density, ρ; (b) isobaric thermal expansivity, α_P; (c) isothermal compressibility, κ_T; and (d) internal pressure, P_i. Symbols as in Figure 2. Arrows indicate increasing temperature.

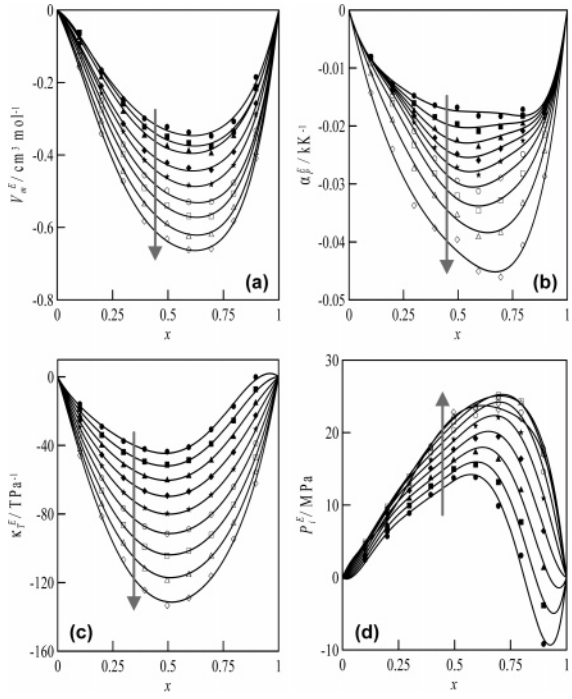

Figure 4. Temperature effect on the isobaric excess properties at $P = 30$ MPa for the x MB + $(1 - x)$ *n*-hexane binary system. (a) Excess molar volume, V_m^E; (b) excess isobaric thermal expansivity, α_P^E; (c) excess isothermal compressibility, κ_T^E; and (d) excess internal pressure, P_i^E. Symbols as in Figure 2. Arrows indicate increasing temperature.

The liquid structure of MB, as for other studied aromatic esters,[8c] is dominated by geometric effects, rising from their size and shape, together with a remarkable dipolar ordering. The almost planar shape of MB molecules (Figure 1) favors an efficient packing in which a close interaction among the MB dipolar moieties is produced; thus, remarkable high densities

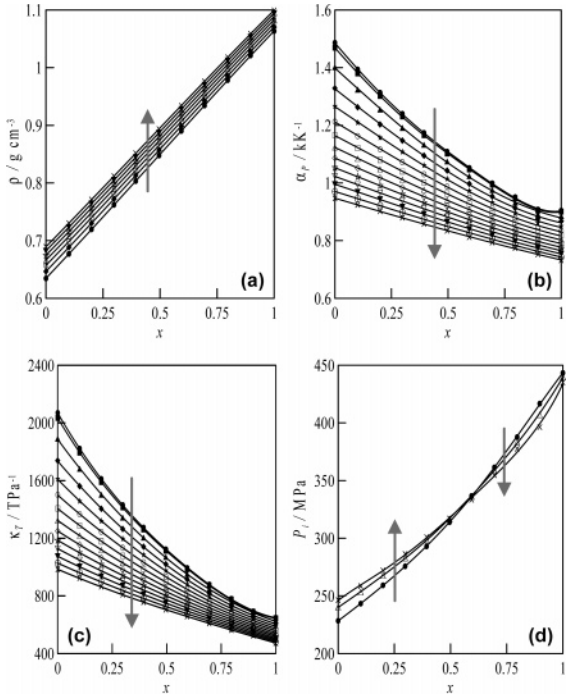

Figure 5. Pressure effect on the isothermal properties at $T = 318.15$ K for the x MB + $(1 - x)$ *n*-hexane binary system. (a) Density, ρ; (b) isobaric thermal expansivity, α_P; (c) isothermal compressibility, κ_T; (d) internal pressure, P_i; (●) 0.1 MPa, (■) 1 MPa, (▲) 5 MPa, (◆) 10 MPa, (★) 15 MPa, (○) 20 MPa, (□) 25 MPa, (△) 30 MPa, (◇) 35 MPa, (☆) 40 MPa, (▽) 45 MPa, (▼) 50 MPa, (⊕) 55 MPa, and (×) 60 MPa. Arrows indicate increasing pressure.

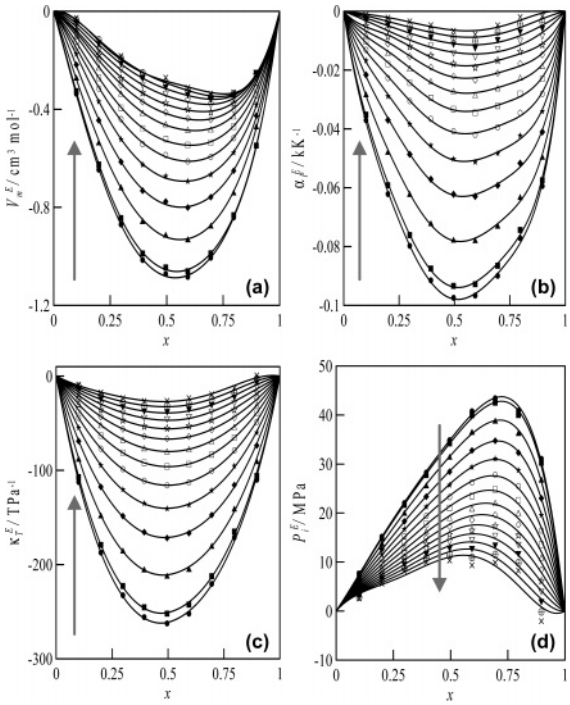

Figure 6. Pressure effect on the isothermal excess properties at $T = 318.15$ K for the x MB + $(1 - x)$ *n*-hexane binary system. (a) Excess molar volume, V_m^E; (b) excess isobaric thermal expansivity, α_P^E; (c) excess isothermal compressibility, κ_T^E; and (d) excess internal pressure, P_i^E. Symbols as in Figure 5. Arrows indicate increasing pressure.

are obtained for this compound. On the other side, HEX is an almost linear molecule with almost null dipole moment and with a liquid structure dominated by weak intermolecular forces of dispersive nature. The mixing process of MB and HEX will be

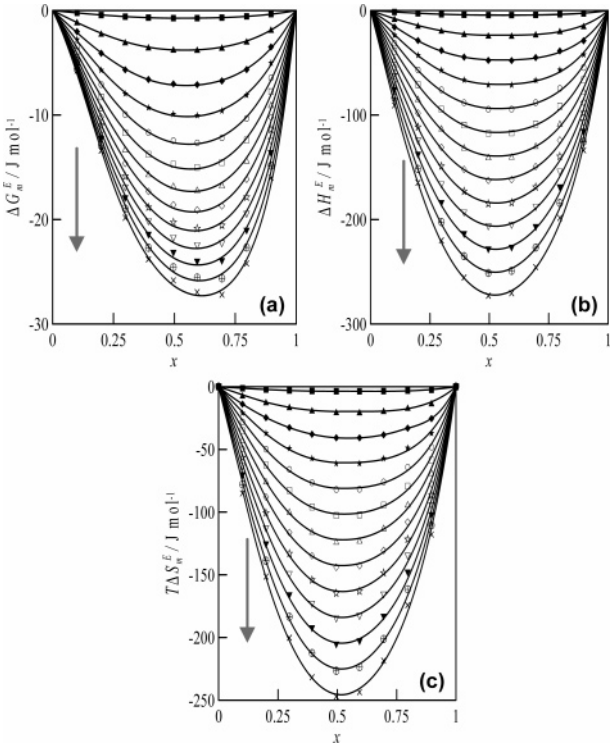

Figure 7. Pressure effect on the isothermal excess properties at $T = 298.15$ K with respect to their values at 0.1 MPa ($\Delta X = X_{298.15,P} - X_{298.15,0.1}$; where X stands for excess Gibbs energy, excess enthalpy, or excess entropy) for the x MB + $(1 - x)$ *n*-hexane binary system. (a) Excess molar Gibbs energy, ΔG_m^E; (b) excess molar enthalpy, ΔH_m^E; and (c) temperature and excess molar entropy factor, $T\Delta S_m^E$. Symbols as in Figure 5. Arrows indicate increasing pressure.

characterized by geometric factors because of the very different shapes of both molecules; the addition of HEX will produce a disruption of the MB local dipolar ordering, but also the linear shape of the HEX molecule will favor an efficient packing of both structures.[10]

The regular behavior of increasing density with decreasing temperature and increasing pressure, Figures 3a and 5a, without maxima or minima, is observed in the reported data with an almost linear behavior for the composition dependence. Isobaric expansivity and isothermal compressibility show also this regular behavior. These last two properties show complex trends. First, from the results, clearly molecular packing in pure MB is much more efficient than in pure HEX, as the stronger pressure and temperature effects on the properties show. For example, isothermal compressibility at 318.15 K decreases 52.5% on going from 0.1 to 60 MPa for pure HEX whereas for MB it decreases 27.5% for the same range. For mixed fluids, as the MB mole fraction increases, the mixtures become less compressible, with weaker pressure and temperature effects on the thermophysical properties, pointing to a more efficient packing. This behavior is in agreement with the negative excess molar volumes, with minima in MB rich regions. The lengths of HEX (8 Å) and MB (7.8 Å) molecules are very close, and thus, both molecules can fit properly. For MB rich regions, the planar shape of ester molecules allows the fitting of linear HEX molecules, giving rise to an efficient packing, although the interaction among MB permanent dipoles should be weakened. HEX rich mixtures are scarcely compact, and thus, although the aromatic ring of MB is voluminous, these molecules can also fit in HEX dominated fluids. The insertion of MB molecules in HEX dominated fluids also weakens the possible interactions of dispersive type among alkane molecules because they require

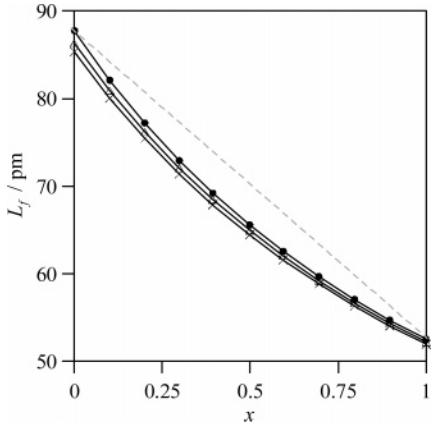

Figure 8. Intermolecular free length, L_f, for the x MB + $(1 - x)$ *n*-hexane binary system at 318.15 K and different pressures. Symbols as in Figure 5. Dashed line shows the linear behavior as a reference.

a close contact among molecules. We should consider that permanent dipole-induced dipole interactions among the ester and the alkane are also possible. These facts are confirmed by negative excess isobaric expansivity and isothermal compressibility, pointing to a mixing process accompanied by a decrease of compressibility, according to the efficient packing that decreases the free volume in the mixture structure. Thus, to confirm the geometric effects in the studied mixtures, the intermolecular free length, L_f, was calculated according to expressions previously reported[8b,26] (Figure 8). L_f is related to fluid free volume because the larger the free volume, the longer the free length. The results reported in Figure 8 show how pure MB is a compact fluid, whereas the free volume in pure HEX is much larger. L_f for mixtures shows a clear deviation from the linear behavior, thus pointing to the aforementioned efficient packing upon mixing.

Internal pressure, reported in Figures 3−6, is a very useful property because it is directly related to the strength of intermolecular forces in the mixtures[27] and because of its relation with Hildebrand solubility parameters. Although the true strength of intermolecular forces is reflected by the so-called cohesive energy density, c, which is related to the vaporization enthalpy, for fluids in which hydrogen bonding is absent or the dipolar moment is lower than 2 D, both properties are almost the same as we have previously reported for MB.[8c] Thus, the lower the internal pressure, the weaker the intermolecular forces. The addition of HEX to MB weakens the intermolecular interactions (Figures 3 and 5), as we may expect from the evolution from dipolar dominated fluids to those in which the prevailing forces are of dispersive nature because of the dominating presence of HEX. The temperature effect on internal pressure shows that increasing values lead to lower internal pressure and thus to weaker interactions. On the contrary, the pressure effect, which is more moderate, shows different trends at low and high MB concentrations. MB rich fluids have compact structures, and thus, an increasing pressure may result in steric hindrance, in which repulsive forces may be remarkable. However, in HEX rich regions, the less compact fluid structures allow a better compression, thus favoring the attractive interactions. Excess internal pressure is positive for almost all the studied temperatures and pressures; negative values are only obtained at high MB concentrations for low temperatures and high pressures.

Excess enthalpy for alkylbenzoate/*n*-alkane mixtures shows strongly endothermic behavior,[28] corresponding to the weakening of intermolecular forces rising from the dipolar dilution of MB dipoles in HEX. The pressure effect on excess enthalpy is reported in Figure 7; increasing pressure produces an exothermic contribution because of the closer proximity among mixture molecules as the pressure rises, thus favoring heteroassociations. Negative pressure contributions for excess Gibbs energy and entropy are also reported. The increasing negative contribution to entropy with increasing pressure shows how the geometrical fitting of both molecules in the mixtures decreases entropy. The negative contribution to excess Gibbs energy as pressure rises shows that the dominating mixture effect is of enthalpic nature for the considered temperatures.

3.2. Molecular Equations of State Modeling. The predictive ability of SAFT[13] and PC-SAFT[14] molecularly based EOS was tested in this work. The EOS characteristics and equations may be found in the original papers, and thus, they are not described here for the sake of brevity. The terminology used for the different model parameters agrees with that used in the original EOS works.[13,14] MB SAFT and PC-SAFT parameters were previously obtained from simultaneous correlation of saturation pressure and saturated liquid density according to a least-squares procedure.[8c] HEX parameters were obtained from the literature.[13,14] The EOS extension to the studied mixtures was done according to a simple monoparametric Berthelot−Lorentz type mixing rule for the crossing terms,[13,14,29] and a single binary interaction parameter, k_{12}, was considered for the whole pressure−temperature range. k_{12} for both EOS was obtained through a least-square procedure of experimental PVT data. Figure 9 shows results of data correlation according to SAFT and PC-SAFT EOS. From the reported data, we may conclude that PC-SAFT gives rise to an excellent data correlation with an average error of 0.51%, thus describing the whole PVT

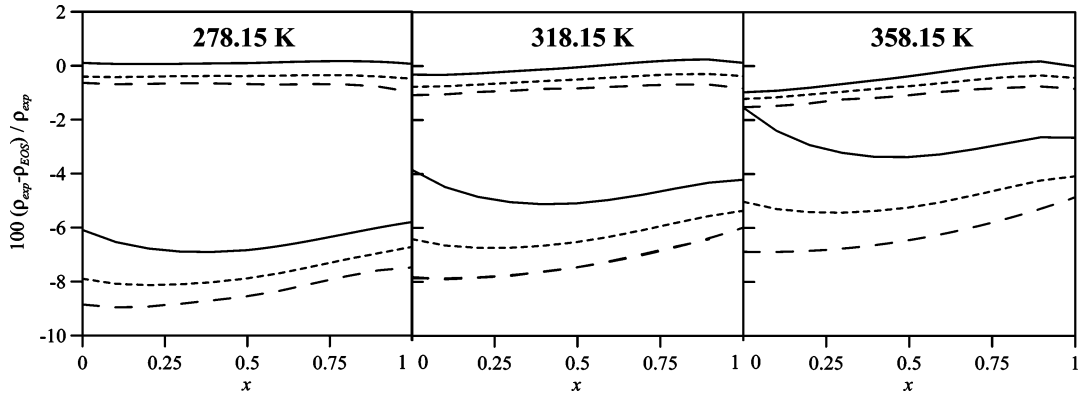

Figure 9. Percentage deviations between experimental and calculated compressed liquid densities at different isotherms for the x MB + $(1 - x)$ *n*-hexane binary system. Calculated data: (top of the panels) PC−SAFT and (bottom of the panels) SAFT; (—) 0.1 MPa, (- - -) 30 MPa, and (— — —) 60 MPa. $k_{12,SAFT} = 0.0213$, $AAD_{SAFT} = 6.07\%$; $k_{12,PC-SAFT} = 0.0025$, $AAD_{PC-SAFT} = 0.51\%$.

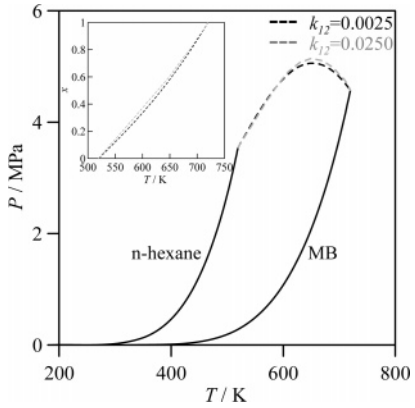

Figure 10. $P-T$ projection of the global phase diagram for the x MB + $(1 - x)$ *n*-hexane binary system. (—) PC−SAFT pure compound properties and (− − −) PC−SAFT (with different k_{12} values) critical locus. The inside plot shows the mole fraction of the critical locus as a function of temperature.

behavior with a single parameter considered as pressure−temperature independent. On the contrary, SAFT correlations are of low quality, and thus, this model should be discarded for these systems as we may expect.

Because of the good performance of the PC-SAFT model, we have predicted the global phase diagram of MB/HEX mixtures with the k_{12} parameter obtained from density correlation (Figure 10). The prediction of phase equilibria using k_{12} parameters obtained from PVT data is not a common practice in the literature, being that the inverse procedure is more frequent. However, the effect of k_{12} on the shape and values of the critical locus is very small (Figure 10). A k_{12} value 10 times greater than the one obtained from PVT optimization does not change neither the type of phase diagram nor the values of the locus. The results obtained show a type I behavior according to the van Konynenburg classification.[30] The predicted critical locus, which is convex upward, shows a maximum at 650 K/5.05 MPa for the k_{12} parameter obtained from PVT optimization with the composition of the critical locus increasing almost linearly. No equilibrium experimental data are available in the literature, and thus, comparison is not possible; considering the accuracy of density predictions, phase equilibria should be predicted with similar accuracy.

3.3. Molecular Dynamics Simulations. We have carried out simulations for five different mixture compositions at three temperatures and three pressures to analyze their effects on mixture properties and structure. Thus, structural and dynamic properties may be analyzed together with predicted macroscopic properties, which will be compared with experimental ones to test the reliability of the molecular model considered for simulations.

The validation of MD simulations, and thus of the considered force field, is done by analyzing the agreement with experimental results for the prediction of thermophysical properties. NPT density predictions obtained in this work are compared with experimental values as a function of composition, temperature, and pressure in Figure 11. An excellent agreement is obtained in the wide temperature−pressure range studied, with deviations always below 2%. The predictive ability of the simulations can be considered as highly satisfactory in spite of the complex mixture structure, with remarkable geometric effects and clustering trends, which are not easily captured by the force field. These accurate predictions, on one hand, show how OPLS-AA is an adequate force field to describe alkylbenzoate/*n*-alkane properties and, on the other hand, show that MD simulations capture the main structural features of these fluids.

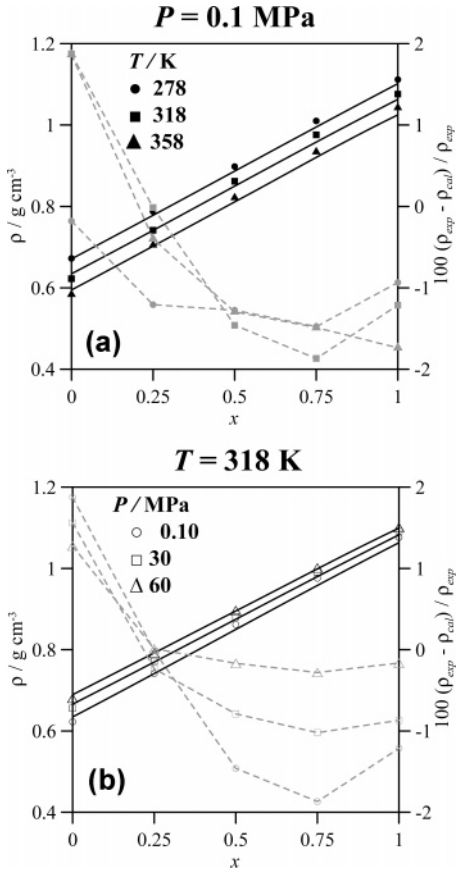

Figure 11. Experimental (continuous lines, Table S1, Supporting Information) and calculated (black symbols, OPLS-AA NPT molecular dynamics) densities for the x MB + $(1 - x)$ *n*-hexane binary system. (a) Temperature effect at 0.1 MPa and (b) pressure effect at 318 K. Percentage errors are also reported. Densities, left axes; percentage errors, right axes; black symbols and continuous lines, densities; gray symbols and dashed lines, percentage errors.

Radial distribution functions, RDFs, provide valuable information on fluid structure, and thus, they are reported in Figures 12−15 in which composition, temperature, and pressure effects on RDFs for selected pairs are analyzed. In Figure 12, composition effect at isothermal/isobaric conditions on RDFs is reported. RDFs for alkylic carbons, C_m-C_m, show a first maximum at 5.25 Å and a second one at 9.55 Å for pure HEX, pointing to two solvation shells. As the MB mole fraction increases, the second maximum moves toward shorter distances, whereas the first one weakens and a shoulder appears leading to a new peak for pure MB. This fact points to an efficient packing of both molecules, which is in agreement with the reported negative excess molar volume. Alkylic chains are closer in the mixtures than in pure HEX because of an efficient mixing process. The remaining RDFs reported in Figure 12 show how the MB liquid structure is affected by the presence of HEX. Surprisingly, almost all the RDFs are clearly reinforced by the presence of the alkane. The interaction among neighbor COO groups is characterized by a first peak in the RDFs around 5 Å ($C-O_c$, $C-O_a$, and O_c-O_a) with positions almost unaffected by the mixture composition; the peaks for these pairs are the largest among all the studied ones. In particular, these peaks are remarkably large for a 25% HEX mixture; the O_c-O_a peak, that shows the position of two highly electronegative atoms (that we should expect to repel each other), is the highest one, then showing proximity of both atoms. In our opinion, this shows the strong clustering tendency of MB in HEX rich solutions, and in this way MB permanent dipoles may interact more

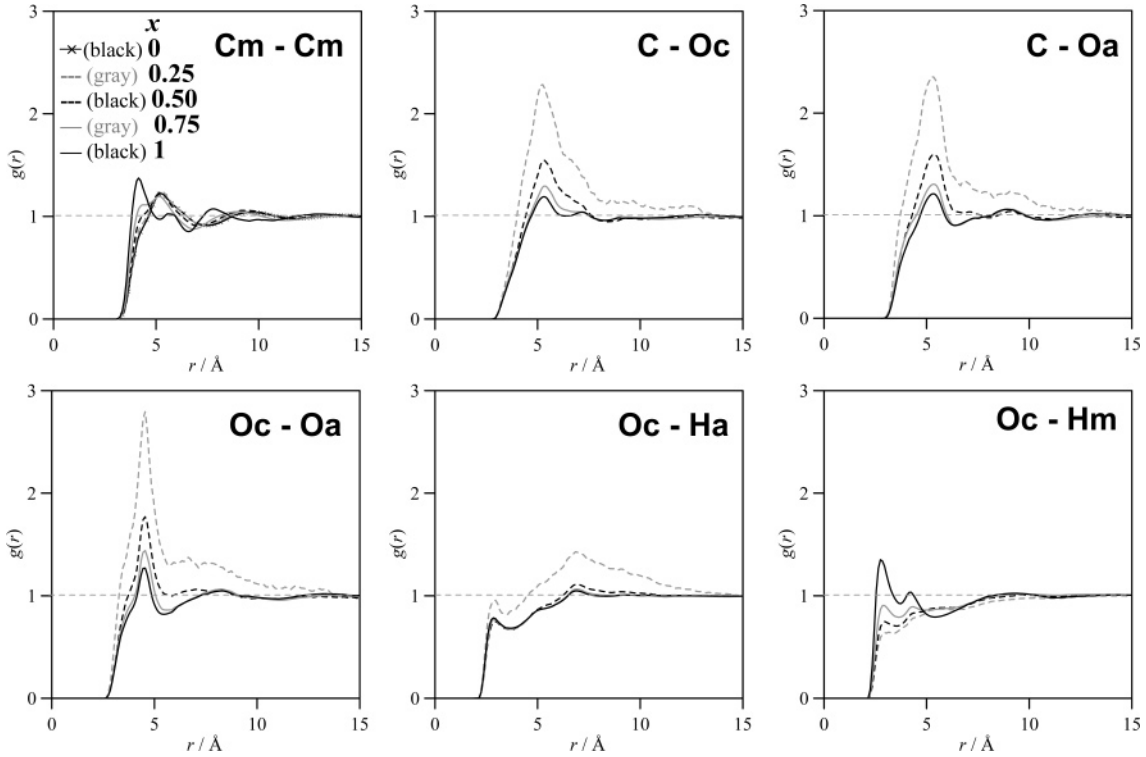

Figure 12. Composition effect on radial distribution functions, $g(r)$, for the x MB + $(1 - x)$ *n*-hexane binary system at 318 K and 0.1 MPa. r = interatomic distance. C = ester group carbon, O_c = carbonyl oxygen, O_a = alkoxy oxygen, C_m = alkylic carbons in MB or *n*-hexane, H_a = hydrogens in the aromatic ring, and H_m = hydrogens in the alkylic chains of MB or *n*-hexane.

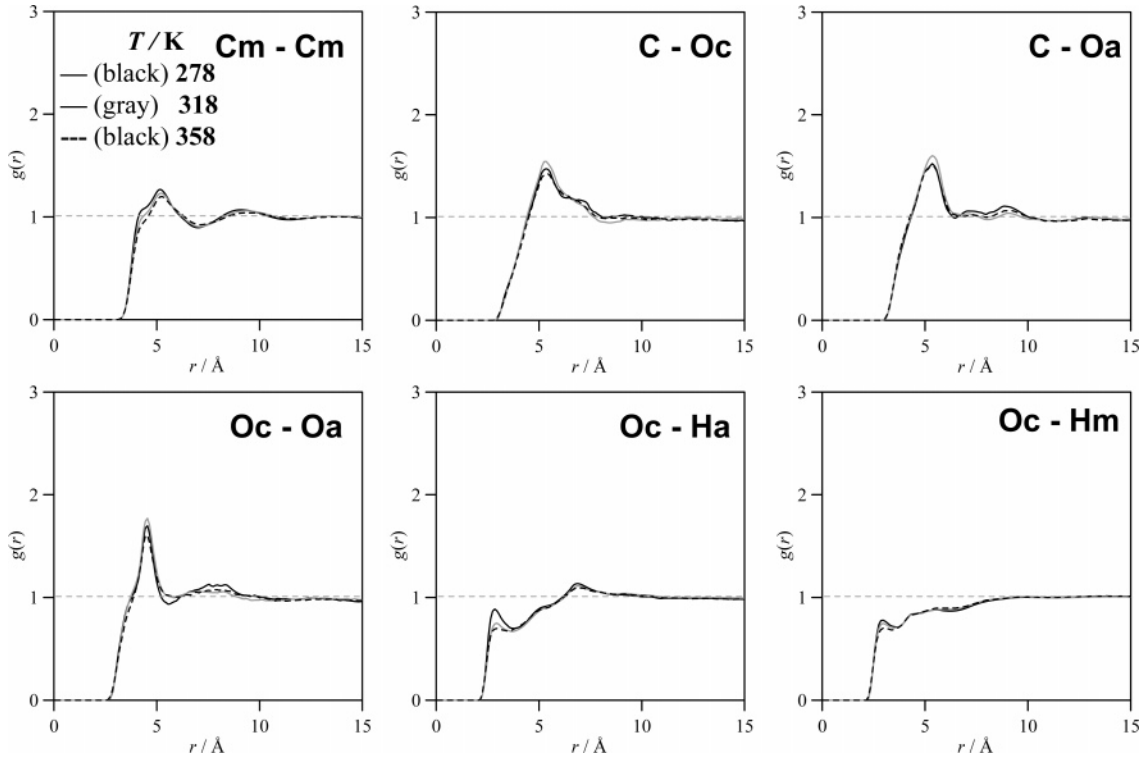

Figure 13. Temperature effect on radial distribution functions, $g(r)$, for the x MB + $(1 - x)$ *n*-hexane binary system for $x = 0.5$ and 0.1 MPa. r = interatomic distance. Labels as in Figure 12.

efficiently, thus keeping the ester molecular groups close to each other. These peaks broaden as the HEX composition increases; thus, whereas for pure MB two solvation shells seem to be present, with increasing HEX mole fraction a single shell with greater radius appears. Thus, a certain MB clustering, forced by the presence of HEX, appears in these mixtures. In a previous work,[8c] we reported a remarkable interaction among carbonyl oxygens and aromatic and alkylic hydrogens in pure MB. In Figure 12, we may see how the interaction with the alkylic hydrogens is clearly weakened upon mixing. However, the interactions with the aromatic hydrogens are almost unaffected, and only at low MB mole fractions they are increased, pointing again to a MB clustering, more remarkable at high HEX mole fractions, in which interactions among carbonyl oxygen and

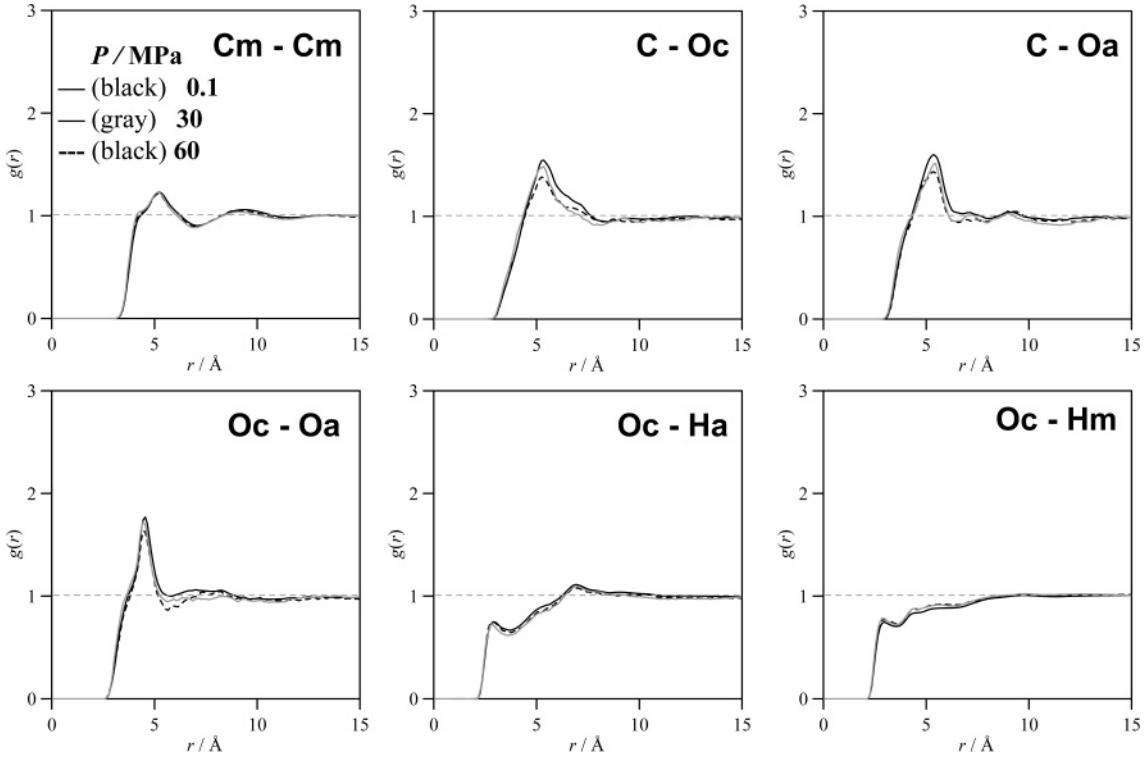

Figure 14. Pressure effect on radial distribution functions, $g(r)$, for the x MB + $(1 - x)$ *n*-hexane binary system for $x = 0.5$ and 318 K. r = interatomic distance. Labels as in Figure 12.

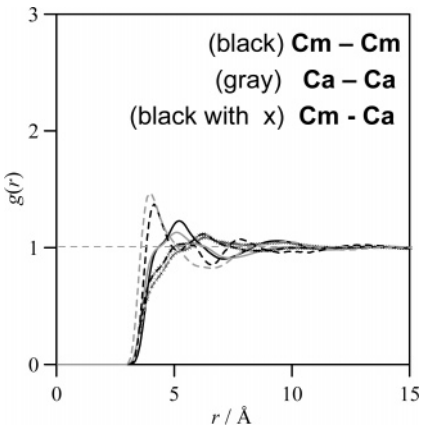

Figure 15. Radial distribution functions, $g(r)$, involving carbon atoms for the x MB + $(1 - x)$ *n*-hexane binary system at 318 K and 0.1 MPa. C_a = aromatic carbons in MB and C_m = alkylic carbons in MB or *n*-hexane. Dashed lines, pure MB; continuous lines, 0.50 MB + 0.50 *n*-hexane.

aromatic hydrogens are reinforced. These results are in agreement with previously reported analysis according to the Kirkwood−Buff theory,[10g] in which a clear like−like preferential solvation was inferred.

The temperature effect on RDFs for isomolar/isobaric conditions is analyzed in Figure 13. The results obtained show a very weak temperature effect in the studied range (278−358 K). RDFs for alkylic carbons are weakened as the temperature rises, with the shoulder in the first peak disappearing and the position of the second maxima moving toward longer distances, thus pointing to a more homogeneous mixture structure with the weakening of apolar domains. RDFs for interactions among carbonyl groups show a complex behavior, whereas the shapes and positions of the maxima are unaffected by the temperature, the first peak is first reinforced and then weakened with rising temperature. Thus, MB clustering is still present at moderate

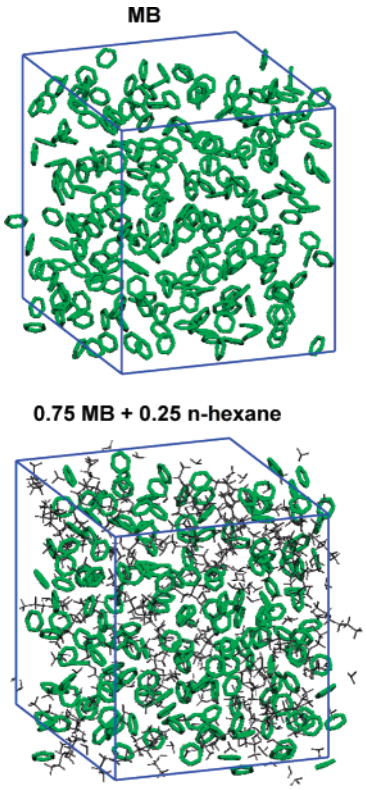

Figure 16. Snapshots showing the spatial arrangement of MB aromatic rings in pure MB and 0.75 MB + 0.25 *n*-hexane mixtures obtained from NPT molecular dynamics simulations at 318 K and 0.1 MPa. Color code for different domains: (green) aromatic rings and (gray) *n*-hexane molecules. Only aromatic rings are plotted for MB molecules.

temperatures and only when the temperature increases remarkably is it weakened and like−like preferential solvation is also weakened. Ester clustering seems to be remarkable in the whole temperature range studied. The interaction among carbonyl

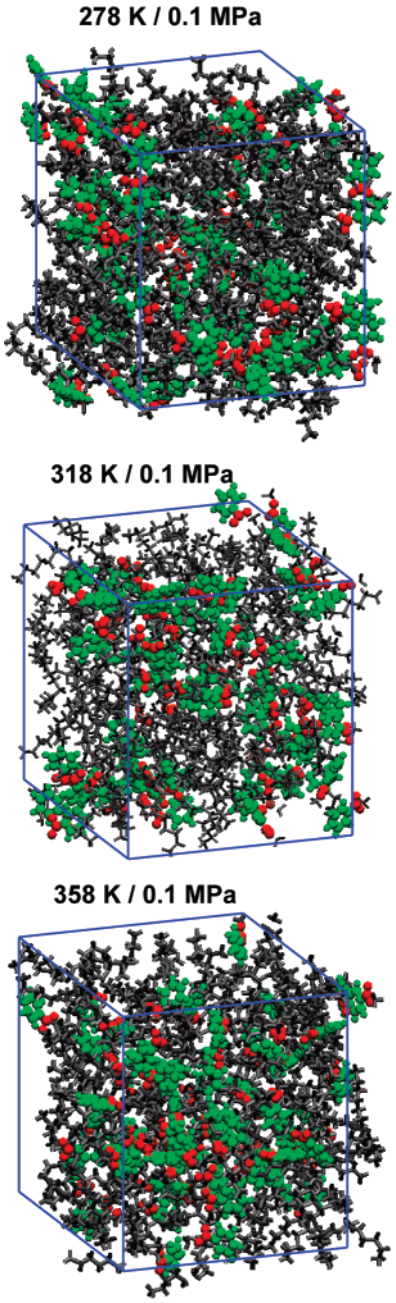

Figure 17. Snapshots for the x MB + $(1 - x)$ *n*-hexane binary system for $x = 0.25$ at different temperatures obtained from NPT molecular dynamics simulations. Color code for different domains: (gray) *n*-hexane molecules, (green) MB aromatic rings, and (red) MB carbonyl groups. *n*-Hexane in sticks representation, MB in balls representation.

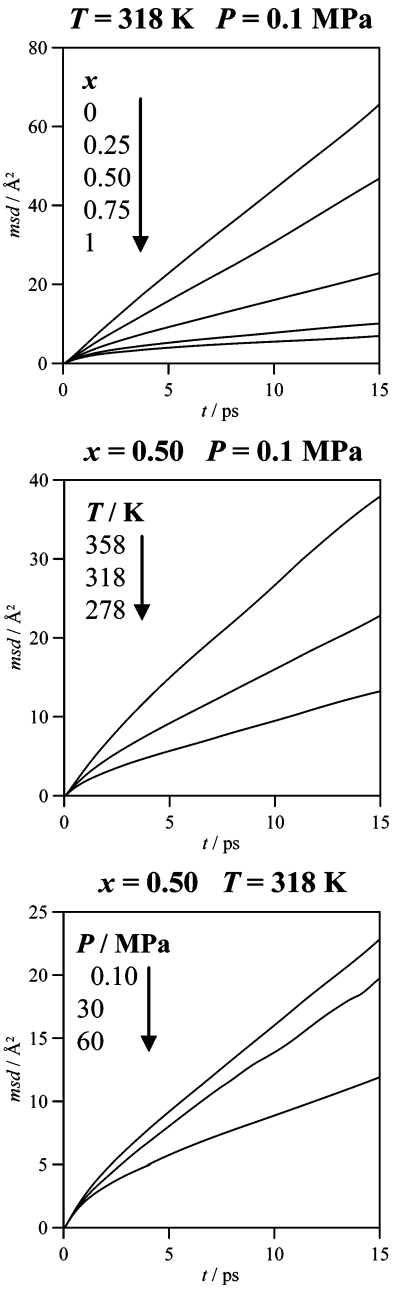

Figure 18. Mean square displacement, msd, for the x MB + $(1 - x)$ *n*-hexane binary system for the first 15 ps of molecular dynamics simulations after equilibration. The values in the panels indicate mole fraction, temperature, and pressure from top to bottom.

oxygen and aromatic or alkylic hydrogens is diminished as temperature rises as we may expect because of the weakening of the MB clustering. Thus, like−like preferential solvation is reinforced as temperature decreases, which is in agreement with previous Kirkwood−Buff results,[10g] pointing to a phase splitting at low temperatures.

Pressure effects on RDFs for isomolar/isothermal conditions is reported in Figure 14. Very weak effects are observed in the broad pressure range studied (0.1−60 MPa). RDFs for the alkylic carbons are almost unaffected by pressure; only the second maximum moves toward lower distances showing slightly more compact consecutive solvation shells but with the presence of apolar domains even at high pressures. The interaction among carbonyl groups is weakened by increasing pressure; all the RDFs diminish as the pressure rises. Pressure decreases like−like preferential solvation and MB clustering, thus approaching the local composition to the bulk one. However, even at the higher-pressure limit, a remarkable interaction among ester groups is present. The decrease of like−like preferential solvation with increasing pressure allows a better contact of MB/HEX molecules, which is in agreement with the pressure effect on excess properties reported in Figure 8.

We report in Figure 15 RDFs for the different carbon atoms that are present in the pure and mixed fluids. For pure MB, there is a clear difference among the packing of aromatic and aliphatic carbons: aromatic carbons are clearly solvated by aliphatic ones, whereas aliphatics may be solvated by both types in a very similar fashion. For mixed MB/HEX fluids, RDFs for aromatic−aromatic carbons do not change, whereas those for aliphatic−aliphatic and aliphatic−aromatic move toward

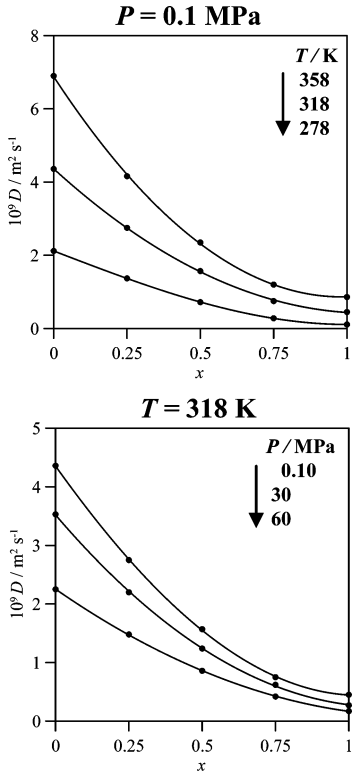

Figure 19. Calculated (OPLS-AA NPT molecular dynamics) self-diffusion coefficient, *D*, for the *x* MB + (1 − *x*) *n*-hexane binary system from msd plots according to Einstein's relation. Solid circles = calculated values, and continuous lines = polynomial fits for guiding purposes. The values in the panels indicate temperature and pressure from top to bottom.

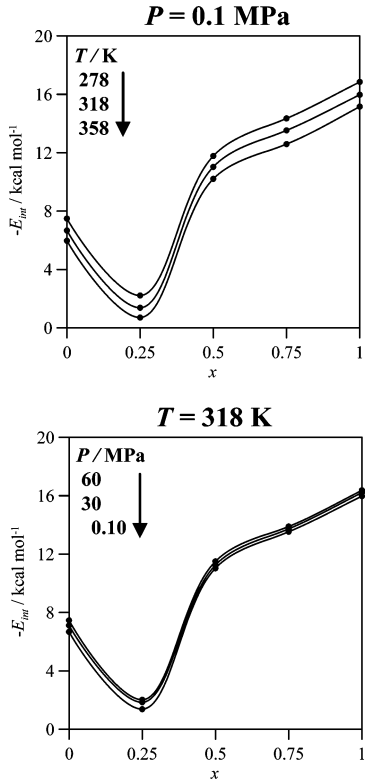

Figure 20. Calculated (OPLS-AA NPT molecular dynamics) intermolecular energy, E_{int}, for the *x* MB + (1 − *x*) *n*-hexane binary system. Solid circles = calculated values, and continuous lines = polynomial fits for guiding purposes. The values in the panels indicate temperature and pressure from top to bottom.

longer distances. Nevertheless, the preferential packing of aromatic carbons by aliphatic ones remains in the mixture.

Another question that arises in the study of these mixtures is the spatial arrangement of aromatic rings and its change upon HEX addition. If we have in mind pure benzene as reference, we may think that aromatic rings in pure MB could stack in T, sandwich, or parallel-displaced configurations. Results reported in Figure 16 for pure MB show that stacking is not produced for this fluid; molecules tend to form angular dispositions with several orientations in the space. This arrangement is in agreement with previously reported ab initio calculations.[8c] This spatial arrangement remains upon HEX addition, hence allowing an efficient fit of HEX molecules.

The snapshot reported in Figure 17 confirms the self-solvation trend in the mixtures with MB forming clusters, in the whole pressure/temperature range studied, and thus with a local composition remarkably different from the bulk one.

Dynamic properties are important and are not easily measurable quantities to characterize fluids. The self-diffusion coefficient, *D*, may be calculated from Einstein's relation:

$$D = \frac{1}{6}\lim_{t\to\infty}\langle \Delta r(t)^2 \rangle \qquad (5)$$

where the quantity in brackets is the mean square displacement msd. It is plotted in Figure 18 as a function of composition, temperature, and pressure for the first 15 ps of the simulation after equilibration with a linear behavior for longer times. The slope of the linear fittings of the msd gives rise to the *D* values reported in Figure 19. The msd decreases with increasing MB mole fraction for isothermal/isobaric conditions, and this is in agreement with the general weakening of intermolecular forces upon mixing considering that pure MB shows stronger forces, of dipolar nature, than pure HEX. The increasing trend of msd with increasing temperature and decreasing pressure is in agreement with the regular behavior of fluids. We should remark that although the msd increases steeply with temperature, the variation with pressure is less regular, showing a slight decrease up to 30 MPa and a stronger variation to 60 MPa. Self-diffusion coefficients for the mixtures reported in Figure 19 could not be compared with experimental values because no data were available. Simulated *D* values for pure HEX are in agreement with experimental ones.[31] Results obtained show how *D* decreases with increasing MB mole fraction for all the studied temperatures and pressures; this effect is more remarkable at high temperatures and pressures, confirming the aforementioned structural results.

Finally, to analyze qualitatively the strength of intermolecular forces in the mixtures, the intermolecular energy calculated from MD simulations is reported in Figure 20. The results show increasing energies as MB mole fraction increases, which is in agreement with the increasing dipolar forces in the mixtures because of the higher dipolar concentration. The remarkable minimum appearing at low MB concentration for all the studied temperatures and pressures shows how the addition of MB disrupts the HEX structure by its trend to self-aggregation and clustering. As the MB mole fraction increases, like−like preferential solvation decreases, and thus, the local composition approaches to the bulk one and intermolecular energy changes almost linearly with composition because of the increasing dipolar concentration.

4. Concluding Remarks

In this paper, a combined experimental and theoretical study on the structure and properties of the MB/*n*-hexane mixed

solvent is reported. The measured PVT surface contributes both to a better understanding of alkylbenzoate containing mixtures structure and to the setting of structure−properties relations, providing a fair set of thermophysical properties needed for industrial applications. The experimental fluid behavior shows an efficient mixture process controlled by geometric effects. Although intermolecular forces are weakened, mainly by dipolar dilution, an efficient packing is produced, giving rise to the remarkably negative excess volume.

The complexity of the mixtures' PVT behavior and structure is not fully captured by the studied molecular-based EOS, for which the predictions are not accurate enough. Only PC-SAFT gives rise to good predictions, whereas SAFT should be discarded for these fluids. The theoretical study shows the existence of a remarkable structural ordering in the fluids, with like−like preferential solvation. This ordering is more remarkable at low MB mole fractions, whereas as the ester concentration rises the local composition approaches the bulk one. The trend of MB to form self-aggregated clusters is also inferred from the simulations. The molecular dynamics study according to the OPLS-AA force field provides a reliable description of the fluid structure and an efficient tool to predict aromatic ester containing mixture properties.

Acknowledgment. Financial support by Junta de Castilla y León, Project BU10/03, and Ministerio de Educación y Ciencia, Project CTQ2005-06611/PPQ (Spain), is gratefully acknowledged.

Supporting Information Available: Tables showing the experimental density (Table S1), TRIDEN fitting coefficients of density (Table S2), isobaric expansibility (Table S3), isothermal compressibility (Table S4), and internal pressure (Table S5) for x MB + $(1 - x)$ *n*-hexane binary mixtures. This material is available free of charge via the Internet at http://pubs.acs.org.

References and Notes

(1) (a) Reichardt, C. *Solvents and Solvent Effects in Organic Chemistry*; Wiley-VCH: Weinheim, 2003. (b) Marcus, Y. *The Properties of Solvents*; Wiley: Chichester, 1998. (c) Buncel, E.; Stairs, R. A.; Wilson, H. *The Role of Solvents in Chemical Reactions*; Oxford University Press: Oxford, U.K., 2003. (d) Rowlinson, J. *Liquids and Liquid Mixtures*; Springer: New York, 1995. (e) Hoheisel, C. *Theoretical Treatment of Liquids and Liquid Mixtures*, Elsevier: Amsterdam, 1992. (f) Hansen, J. P.; McDonald, I. R. *Theory of Simple Liquids*; Academic Press: London, 2003.

(2) Archer, W. L. *Industrial Solvents Handbook*; Marcel Dekker: New York, 1996.

(3) (a) Seider, W. D.; Seader, J. D.; Lewin, D. R. *Product and Process Design Principles: Synthesis, Analysis, and Evaluation*; John Wiley: New York, 2003. (b) Sikdar, S. *Process Design Tools for the Environment*; CRC: Boca Raton, FL, 2001.

(4) Dohrn, R.; Pfohl, O. *Fluid Phase Equilib.* **2002**, *15*, 194−197.

(5) Raal, J. D.; Muhlbauer, A. L. *Phase equilibria. Measurement and computation*; Taylor and Francis: New York, 1998.

(6) (a) Sandler, S. I. *Fluid Phase Equilib.* **2003**, *210*, 147. (b) Prausnitz, J. M.; Lichtenthaler, R. N.; Gomes de Azevedo, E. *Molecular Thermodynamics of Fluid Phase Equilibria*; Prentice Hall: Upper Saddle River, NJ, 1998. (c) Heyes, D. M. *The Liquid State: Applications of Molecular Simulations*; Wiley: Chichester, 1998. (d) Sadus, R. J. *Molecular Simulation of Fluids*; Elsevier: Amsterdam, 1999.

(7) (a) Berry, R. S.; Rice, S. A.; Ross, J. *Matter in Equilibrium: Statistical Mechanics and Thermodynamics*; Oxford University Press: Oxford, U.K., 2001. (b) Kazantzi, V.; Qin, X.; El-Halwagi, M.; Eljack, F.; Eden, M. *Ind. Eng. Chem. Res*. **2007**, *46*, 3400. (c) Eljack, F. T.; Eden, M. R.; Kazantzi, V.; Qin, X.; El-Halwagi, M. M. *AIChE J.* **2007**, *53*, 1232.

(8) (a) Dávila, M. J.; Aparicio, S.; Alcalde, R.; García, B.; Leal, J. M. *Green Chem*. **2007**, *9*, 221. (b) Aparicio, S.; Alcalde, R.; Dávila, M. J.; García, B.; Leal, J. M. *J. Phys. Chem. B* **2007**, *111*, 3167. (c) Aparicio, S.; Alcalde, R.; Dávila, M. J.; García, B.; Leal, J. M. *J. Phys. Chem. B* **2007**, *111*, 4417.

(9) (a) Tsierkezos, N. G.; Kelarakis, A. E.; Molinou, I. E. *J. Chem. Eng. Data* **2000**, *45*, 776. (b) Semeniuk, B.; Wilczura-Wachnick, H. *Fluid Phase Equilib.* **1998**, *152*, 337. (c) Ortega, J.; Postigo, M. A. *Fluid Phase Equilib.* **1995**, *108*, 121. (d) García, B.; Ortega, J. C. *J. Chem. Eng. Data* **1988**, *33*, 200. (e) García, B.; Ortega, J. C. *Thermochim. Acta* **1987**, *117*, 219. (f) Aminabhavi, T. M.; Raikar, S. K. *Collect. Czech. Chem. Commun*. **1993**, *58*, 1761. (g) Aminabhavi, T. M.; Phayde, H. T. S.; Khinnavar, R. S.; Gopalakrishna, B. *J. Chem. Eng. Data* **1994**, *39*, 251. (h) Dusart, O.; Piekarski, C.; Piekarski, S.; Viallard, A. *J. Chim. Phys. Phys. Chim. Biol.* **1976**, *73*, 837. (i) Grolier, J. P. E.; Ballet, D.; Viallard, A. *J. Chem. Thermodyn.* **1974**, *6*, 895.

(10) (a) García, B.; Alcalde, R.; Aparicio, S.; Leal, J. M. *Ind. Eng. Chem. Res.* **2002**, *41*, 4399. (b) García, B.; Alcalde, R.; Aparicio, S.; Leal, J. M. *Phys. Chem. Chem. Phys.* **2002**, *4*, 5833. (c) García, B.; Aparicio, S.; Alcalde, R.; Leal, J. M. *J. Phys. Chem. B* **2003**, *107*, 13478. (d) García, B.; Aparicio, S.; Navarro, A. M.; Alcalde, R.; Leal, J. M. *J. Phys. Chem. B* **2004**, *108*, 15841. (e) Aparicio, S.; Alcalde, R.; Leal, J. M.; García, B. *J. Phys. Chem. B* **2005**, *109*, 6375. (f) Aparicio, S.; Alcalde, R.; García, B.; Leal, J. M. *Ind. Eng. Chem. Res.* **2005**, *44*, 7575. (g) Alcalde, R.; Aparicio, S.; García, B.; Leal, J. M. *J. Phys. Chem. B* **2005**, *109*, 19908.

(11) Sengers, J. V., Kayser, R. F., Peters, C. J., White, H. J., Eds. *Equations of State for Fluids and Fluid Mixtures*; Elsevier: Amsterdam, 2000.

(12) Wertheim, M. S. *J. Chem. Phys.* **1986**, *85*, 2929.

(13) (a) Chapman, W. G.; Gubbins, K. E.; Jackson, G.; Radosz, M. *Fluid Phase Equilibr*. **1989**, *52*, 31. (b) Chapman, W. G.; Gubbins, K. E.; Jackson, G.; Radosz, M. *Ind. Eng. Chem. Res*. **1990**, *29*, 1709. (c) Huang, S. H.; Radosz, M. *Ind. Eng. Chem. Res.* **1990**, *29*, 2284.

(14) Gross, J.; Sadowski, G. *Ind. Eng. Chem. Res.* **2001**, *40*, 1244.

(15) Jorgensen, W. L.; Maxwell, D. S.; Tirado-Rives, J. *J. Am. Chem. Soc.* **1996**, *118*, 11225.

(16) (a) García, B.; Aparicio, S.; Alcalde, R.; Dávila, M. J.; Leal, J. M. *Ind. Eng. Chem. Res.* **2004**, *43*, 3205. (b) Aparicio, S.; García, B.; Alcalde, R.; Dávila, M. J.; Leal, J. M. *J. Phys. Chem. B* **2006**, *110*, 6933.

(17) Lemmon, E. W.; McLinden, M. O.; Friend, D. G. Thermophysical Properties of Fluid Systems. In *NIST Chemistry WebBook, NIST Standard Reference Database Number 69*; Linstrom, P. J., Mallard, W. G., Eds.; National Institute of Standards and Technology: Gaithersburg, MD, 2005; http://webbook.nist.gov.

(18) Ponder, J. W. *TINKER: Software tool for molecular design*, version 4.2; Washington University School of Medicine: St. Louis, MO, 2004.

(19) Hoover, W. G. *Phys. Rev. A* **1985**, *31*, 1695.

(20) Allen, M. P.; Tildesley, D. J. *Computer Simulation of Liquids*; Clarendon Press: Oxford, U.K., 1989.

(21) Rickaert, J. P.; Ciccotti, G.; Berendsen, H. J. *J. Comput. Phys*. **1977**, *23*, 327.

(22) Essmann, U. L.; Perera, M. L.; Berkowitz, T.; Darden, H.; Lee, H.; Pedersen, L. G. *J. Chem. Phys.* **1995**, *103*, 8577.

(23) (a) Martínez, J. M.; Martínez, L. *J. Comput. Chem*. **2003**, *24*, 819. (b) Friedlander, A.; Martínez, J. M.; Santos, S. A. *Appl. Math. Optim*. **1994**, *30*, 235.

(24) Besler, B. H.; Merz, K. M.; Kollman, P. A. *J. Comput. Chem.* **1990**, *11*, 431.

(25) Ihmehls, E. C.; Gmehling, J. *Ind. Eng. Chem. Res*. **2001**, *40*, 4470.

(26) Pandey, J. D.; Dey, R.; Chhabra, J. *Phys. Chem. Commun.* **2003**, *6*, 55.

(27) Dack, M. R. J. *Chem. Soc. Rev.* **1975**, *4*, 211.

(28) (a) Ortega, J.; Postigo, M. A. *Fluid Phase Equilib.* **1995**, *108*, 121. (b) Blanco, A. M.; Ortega, J. *Int. J. Thermophys*. **1994**, *15*, 699. (c) Grolier, J. P. E.; Ballet, A.; Viallard, A. *J. Chem. Thermodyn*. **1974**, *6*, 895.

(29) Aparicio, S.; Hall, K. R. *Ind. Eng. Chem. Res.* **2007**, *46*, 273.

(30) Van Konynenburg, P. H.; Scott, R. L. *Philos. Trans. R. Soc. London, Ser. A* **1980**, *298*, 495.

(31) Harris, K. R. *J. Chem. Soc., Faraday Trans. 1* **1982**, *78*, 2265.